Alexandria Engineering Journal (2015) 54, 373–382

HOSTED BY

Alexandria University

Alexandria Engineering Journal

www.elsevier.com/locate/aej
www.sciencedirect.com

ORIGINAL ARTICLE

Effective reduction of in-cylinder peak pressures in Homogeneous Charge Compression Ignition Engine – A computational study

T. Karthikeya Sharma *, G. Amba Prasad Rao, K. Madhu Murthy

Department of Mechanical Engineering, NIT Warangal, 506004 TS, India

Received 12 January 2015; revised 9 April 2015; accepted 15 April 2015
Available online 2 May 2015

KEYWORDS

HCCI engine;
ECFM-3Z;
Swirl ratio;
Peak pressures;
EGR;
Compression ratio

Abstract HCCI mode of combustion is known for simultaneous reduction of NOx and PM emissions besides yielding low specific fuel consumption. The nature of volumetric combustion of HCCI engine leads to the development of high peak pressures inside the combustion chamber. This high peak pressures may damage the engine, limiting the HCCI engine life period and thus demands sturdy designs. In this study an attempt is made to analyze computationally the effect of induction swirl in reducing the peak pressures of a HCCI engine under various operating parameters. For the study, specifications of a single cylinder 1.6 L, reentrant piston bowl diesel engine are chosen. For the computational analysis ECFM-3Z model of STARCD is considered. This model is suitable to analyze the combustion processes in SI and CI engines. As HCCI engine is a hybrid version of SI and CI engines, ECFM-3Z model with necessary modifications is used to analyze the peak pressures inside the combustion chamber. The ECFM-3Z model for HCCI mode of combustion is validated with the existing literature to make sure that the results obtaining are accurate. Numerical experiments are performed to study the effect of compression ratio, equivalence ratio, exhaust gas recirculation and boost pressure under different swirl ratios in reducing the in-cylinder peak pressures. The results showed that swirl ratio has a considerable impact in limiting the peak pressures of HCCI engine. The analysis resulted in achieving about 21% reduction in peak pressures are achieved when a swirl ratio of 4 with 30% EGR is adopted when compared to a swirl ratio of 1 with 0% EGR. The study revealed that out of the four operating parameters selected, lower compression ratios, higher EGR concentrations, lower equivalence ratios, lower boost pressures and higher swirl ratios are favorable in reducing the peak pressures.

1. Introduction

The Homogeneous Charge Compression Ignition (HCCI) is considered to be the principally promising future IC engine combustion concepts. HCCI is a concept of hybrid

* Corresponding author.
Peer review under responsibility of Faculty of Engineering, Alexandria University.

http://dx.doi.org/10.1016/j.aej.2015.04.006
1110-0168 © 2015 Faculty of Engineering, Alexandria University. Production and hosting by Elsevier B.V.

combustion, between conventional combustion concepts of spark ignition engine and compression ignition engine. HCCI concept is however not a modern finding. Already in the early twentieth century hot bulb engines operated with an HCCI-like combustion. They were superior in terms of brake thermal efficiency compared with the contemporary gasoline engines and at the same level as the diesel engines. Research has revealed that high engine efficiencies, ultra low NO emissions and low particulates are the benefits of HCCI engines. Volumetric autoignited combustion of the compressed lean air–fuel mixture is attributed to these benefits. Though HCCI concept is attractive, it suffers from few limitations such as low specific output, narrow operating range, lack of control over the ignition process, long start-up time and high levels of CO and UHC emissions. The CO and UHC emissions can be after treated using catalytic converters [1–3]. Heywood et al. explained the combustion characteristics of HCCI combustion along with the many other fundamental concepts about the combustion in an IC engine. Heywood reported that the problems such as high particulate matter and soot emissions (because of fuel rich and diffusion rich regions) associated with the conventional CI engine can be overcome by HCCI engines. Volumetric combustion and low temperature combustion of HCCI engine resulted in low particulate and soot formations. Also, low specific fuel consumption was the most attractive of HCCI engines when compared with the conventional CI engines [4]. Onishi et al. conducted experiments to visualize the process of combustion on a conventional SI engine in both SI and HCCI modes using schlieren photography method. From their experimental results they reported that very wee defined propagation of flame was found in SI operation mode but no visible propagation of flame was found in HCCI mode of combustion; proving volumetric combustion of HCCI engines [5,6].

Chen et al. numerically investigated the effect of EGR in reducing the pressure rise rate in HCCI engine. They incorporated CHEMKIN and SENKIN code for the analysis. They reported that with increase in EGR fraction retarded the start of combustion and decreased the peak pressure and temperature rise. Under the same conditions with increase in EGR ratio, extension in preparation of thermal ignition and advancement in LTHR timing were observed [7].

Swirl helps in homogeneous mixture formation of the fuel and air [8]. It also helps in NOx emission reduction [9]. The increase in swirl ratio reduces the peak temperatures by increasing the heat transfer to the combustion chamber parts. This leads to a low temperature combustion process resulting in low NOx emissions [10].

Performing these explorations (under different operating parameters with induction induced swirl) solely in the laboratory would be expensive, inefficient and impractical because of the complex interactions of the many variables. Because of this reason, a CFD tool Star-CD is chosen for the analysis. Several modifications were made to Star-CD es-ice module so that it could be used for HCCI engine modeling. Many commercial CFD packages such as Open FOAM, Ricardo Wave, GT Power, AVL FIRE are available to simulate the combustion process in IC engines. In the present work "es-ice" of STAR-CD is used for the analysis. The various models developed for presaging the engine combustion processes are Transient Interactive Flamelets (TIF) model, Digital Analysis of Reaction System-Transient Interactive Flamelets model (DARS-TIF), G-equation model, Extended Coherent Flame Combustion Model-3 Zones [11,12] and the Equilibrium-Limited ECFM (ECFM-CLEH) [13,14]. Each combustion model possesses limitations and advantages and is appropriate for a particular set of problems. In general ECFM-CLEH and ECFM-3Z are suitable for almost all types of combustion regimes, but ECFM-3Z is mainly applicable for premixed homogeneous turbulent combustion with both SI and CI. Table 1 shows the applicabilities of the various combustion models. Due to its vast range of suitability, ECFM-3Z has been used in the present investigation to examine the impact of piston bowl geometry on flow and combustion characteristics. Fig. 1 shows the schematic representation of the three zones of the ECFM-3Z model.

Induction induced swirl has a predominant effect on mixture formation and rapid spreading of the flame front in the conventional combustion process of a CI engine. This has been well documented in the literature. However, it is observed that no work has been done on the effect of swirl in HCCI mode.

The main objective of the present study was to analyze the effect of induction induced swirl in reducing the peak pressures of the HCCI engine under varying operating parameters. Because of the volumetric combustion the development of peak pressures inside the combustion chamber is very high. This is one of the limitations of the HCCI engine which demands the rigid body construction of the engine and reduces the engine life. In this regard a computational attempt is made to control the peak pressures in terms of induction induced swirl along with other parameters.

2. Methodology

A DI single cylinder CI engine with two different piston bowls was considered for the analysis. The specifications of the engine are tabulated in Table 2 have been considered for the analysis. Reentrant and spherical piston bowls are taken. Care was taken to have same clearance volume with all the two piston bowls. To study the parameters such as flame distribution inside the combustion chamber, rates of heat release, temperatures, pressures and emissions of NO and CO a multidimensional CFD package of STAR-CD; ECFM-3Z is used. The model of the piston bowl shaper was prepared and meshed as per the specification without having any variation in the compression ratio. The analysis was started with a starting angle of 680° CA and ending angle of 800° CA.

3. CFD model set-up

A spline was created in the shape of the piston bowl and was transformed into a 2D template. The 2D template was then cut into 3D piston bowl representing 1/6th of the piston bowl. The 1/6 piston bowl computational mesh has around 128,000

Table 1 Combustion model capabilities.

Model	Applicability
G-Equation	Partially premixed SI and CI
DARS-TIF	Compression ignition
ECFM	Non-homogeneous premixed SI
ECFM-3Z	Premixed and nonpremixed SI and CI

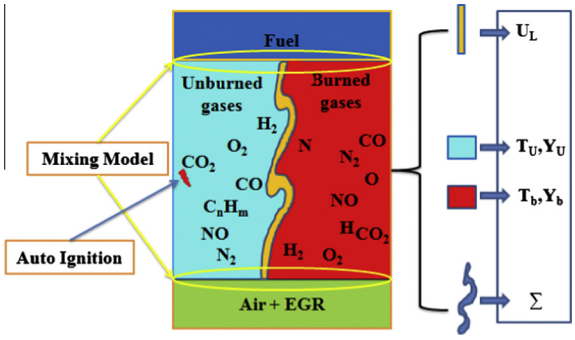

Figure 1 Schematic representation of three zones of ECFM-3Z model.

cells BDC, and 52,000 cells at TDC with tetrahedral cells. By comparing the peak pressure results with a finer grid having 12,400–259,000 cells a grid independence study was performed. The numerical results represented that the peak pressure values are almost constant after 128,000 representing grid independent nature, but with higher computational processing time. Hence, the optimal cell size of 128,000 is considered for the analysis. The 3D mesh consists of 40 radial cells, 160 axial cells, 5 top dead center layers and 40 axial block cells. The grid independent analysis representing In-cylinder pressures vs Number of cells is represented in Fig. 2a. The piston bowl shape and 3D mesh of the piston bowl sector is shown in Fig. 2b and c.

Gross indicated Work per cycle (W) is used to analyze the engines energy efficiency which is calculated from the displacement of the piston and pressure in the cylinder using Eq. (1):

$$W(\mathrm{N\ m}) = \frac{\pi a B_2}{8} \int_{\theta_1}^{\theta_2} p(\theta) \left[2\sin(\theta) \frac{a\sin(2\theta)}{\sqrt{l^2 - a^2\sin^2(\theta)}} \right] d\theta \qquad (1)$$

where a = crank radius, l = length of the connecting, B = bore of the cylinder, and θ_1 and θ_2 are the beginning and the end of the valve-closing period.

The relation between indicated work per cycle and indicated power per cylinder (P) is shown in Eq. (2):

$$P(\mathrm{kW}) = \frac{WN}{60,000 n_R} \qquad (2)$$

Table 2 Engine specifications.

Engine specifications	
Displacement volume	1600 cm^3
Bore	12.065 cm
Stroke	14 cm
Connecting rod length	26 cm
Compression ratio	21:1
Fuel	*n*-Dodecane
Operating conditions	
Engine speed	1000 rpm
Equivalence ratio	0.26
Inlet temperature air (T_{air})	353 K
Inlet air pressure (P_{air})	0.1 MPa
Cylinder wall temperature (T_{wall})	450 K
EGR	0%

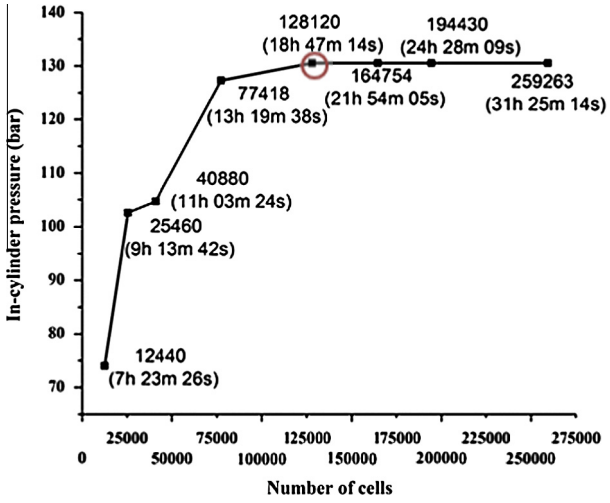

Figure 2a Grid independent study.

where n_R is taken as 2 is the no. of revolutions of the crank for power stroke per cylinder and N is the speed of the engine (rpm). The indicated specific fuel consumption (ISFC) is shown in Eq. (3):

$$\mathrm{ISFC(g/kW\ h)} = \frac{30 m_{\mathrm{fuel}} N}{P} \qquad (3)$$

In Eqs. 1–3 the power and ISFC analyses are qualitative only.

4. Modeling strategy

STAR-CD is a combined package consisting of several sub-models to simulate all the SI and CI engine computations. The sub-model such as atomization and fuel spray, turbulence (I–L), boundary wall function, NOx, auto-ignition, combustion (ECFM-3Z), was included in the STAR-CD es-ice package. Ideal gas laws and C_p as a function of temperature are chosen to deal with fluid properties.

4.1. Swirl creation

The swirl inside the combustion chamber is generated by varying the intake charge velocity components in U and V directions. The velocity components of U and V are calculated as follows.

$$U = -(x - x_{\mathrm{CSYS}})(\mathrm{Swirl} \cdot \mathrm{RPM} \cdot 2\pi)/60 \qquad (4)$$

$$V = -(y - y_{\mathrm{CSYS}})(\mathrm{Swirl} \cdot \mathrm{RPM} \cdot 2\pi)/60 \qquad (5)$$

where U and V are the intake charge velocity components in X and Y directions. RPM is the engine speed. x, x_{CSYS} y, y_{CSYS} are the x and y Global and local coordinates. The local and global coordinates Z axis is to be matched after meshing to eliminate error.

4.2. Spray injection and atomization model

Huh's [15,16] model is useful in modeling spray and atomization processes in conventional CI engines. Nozzle generated the turbulence stresses, and gas inertia are the mechanisms involved in Huh's model to deal with spray and atomization.

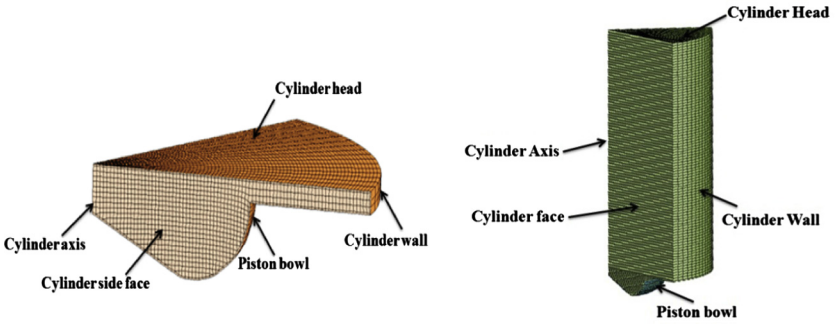

(b) @ TDC (c) @ BDC

Figure 2b and c Schematic representation of 3D piston bowl shape at TDC and BDC.

The turbulence generated in the nozzle during the jet leaving the nozzle hole develops a surface wave growth direct toward formation of droplets.

Secondary break-up of the droplets takes place because of continuous phasing and non-uniform pressure around the droplet. The secondary break-up is mainly depended on Weber number (We_d) and the dimensionless droplet diameter d^* as shown in Eq. (6): Reitz–Diwakar model [17,18] is used in computing the secondary break-up of the droplets.

$$We_d = \frac{\rho_d D_d V_{d,n}^2}{\sigma} \tag{6}$$

where 'n' = unit normal to the wall, '$V_{d,n}$' = the velocity normal component normal to the wall, 'σ' = surface tension coefficient.

Premixed mechanism is considered for HCCI mode to prepare a fuel and air homogeneous mixture.

4.3. Autoignition model

Instead pre-ignition kinetics, ignition occurrence time is established to compute time of the delay in Ignition.

The auto-ignition delay τ_d is computed using Eq. (7):

$$\tau_d = 1.051 \times 10^{-8}[\mathrm{F}]^{0.05}[\mathrm{O_2}]^{-0.53}\rho^{0.13}\mathrm{e}^{5914/T\mu}[47/\mathrm{CN}] \tag{7}$$

where CN = cetane number (max = 60). To track the reactions development an ignition progress variable function is defined as shown in Eq. (8):

$$(dY_{\mathrm{igi}})/(dt) = Y_{\mathrm{Tf}}F(\tau_d) \tag{8}$$

As HCCI mode of combustion is controlled by cool flames a double delay auto-ignition model is used. The reaction rates slowed down because of low temperatures in cool flame regime. Main-auto-ignition starts because of the increased rates of reaction after second delay.

The double delay auto-ignition model deals with two ignition progress variables and two nonempirical precomputed delay times. It is possible to estimate the maximum fuel burnt at each auto-ignition step from these ignition progress variables.

4.4. Combustion model

A Three Zone Extended Coherent Flame Combustion Model (EFCM-3Z) is used to simulate the HCCI mode of combustion. Auto-ignition of the premixed fuel and air takes place because of high temperatures generated at the end of the compression stroke in HCCI mode. The ECFM-3Z model is capable of dealing with propagation of flame, turbulence, double delay auto-ignition, postflame models and emissions of the modern HCCI engines. Angelberger et al. [19] wall function model was used to resolve the wall-bounded flows; turbulence generated near-wall region. The turbulent and molecular lever mixing of gases in the two zones called unmixed fuel zone and unmixed (air + EGR zone) forms a mixing zone and where the combustion takes place.

The mass fractions of the unmixed fuel (Y_{fum}) can be obtained from Eq. (9):

$$\frac{\partial \rho Y_{fum}}{\partial t} + \nabla \cdot (\rho u Y_{fum}) - \nabla \cdot \left[\left(D + \frac{\mu_t}{SC_t}\right)\nabla Y_{fum}\right] = \frac{\beta_{m_{in}}}{\pi} Y_{fum}\left(1 - Y_{fum}\frac{\rho}{\rho_u}\frac{w_m}{w_f}\right) + \dot{\omega}_e Vap \tag{9}$$

4.5. NO_x model

The reaction of N_2 of the air with O_2 in the combustion leads to the formation of NOx emissions. Usually this reaction occurs at high temperatures generated because of combustion. The emissions of NOx are highly sensitive to higher temperatures and are directly related. Prompt and thermal NOx are the two sources for NOx emissions from an IC engine. Thermal NOx emissions are in major portions from the diesel engine NOx emissions. To model NOx emissions Extended Zel'dovich mechanism [20] is considered. The Extended Zel'dovich mechanism deals with the below equations by Bowman [20]

$$\mathrm{O} + \mathrm{N_2} \leftrightarrow \mathrm{NO} + \mathrm{N} \tag{10}$$

$$\mathrm{N} + \mathrm{O_2} \leftrightarrow \mathrm{NO} + \mathrm{O} \tag{11}$$

$$\mathrm{N} + \mathrm{OH} \leftrightarrow \mathrm{NO} + \mathrm{H} \tag{12}$$

With the partial equilibrium of Eq. (12) for the hydrogen radicals,

$$\mathrm{O} + \mathrm{OH} \leftrightarrow \mathrm{O_2} + \mathrm{H} \tag{13}$$

Heywood [21] developed a single NO rate equation to represent the Extended Zeldovich mechanism and is shown in Eq. (14):

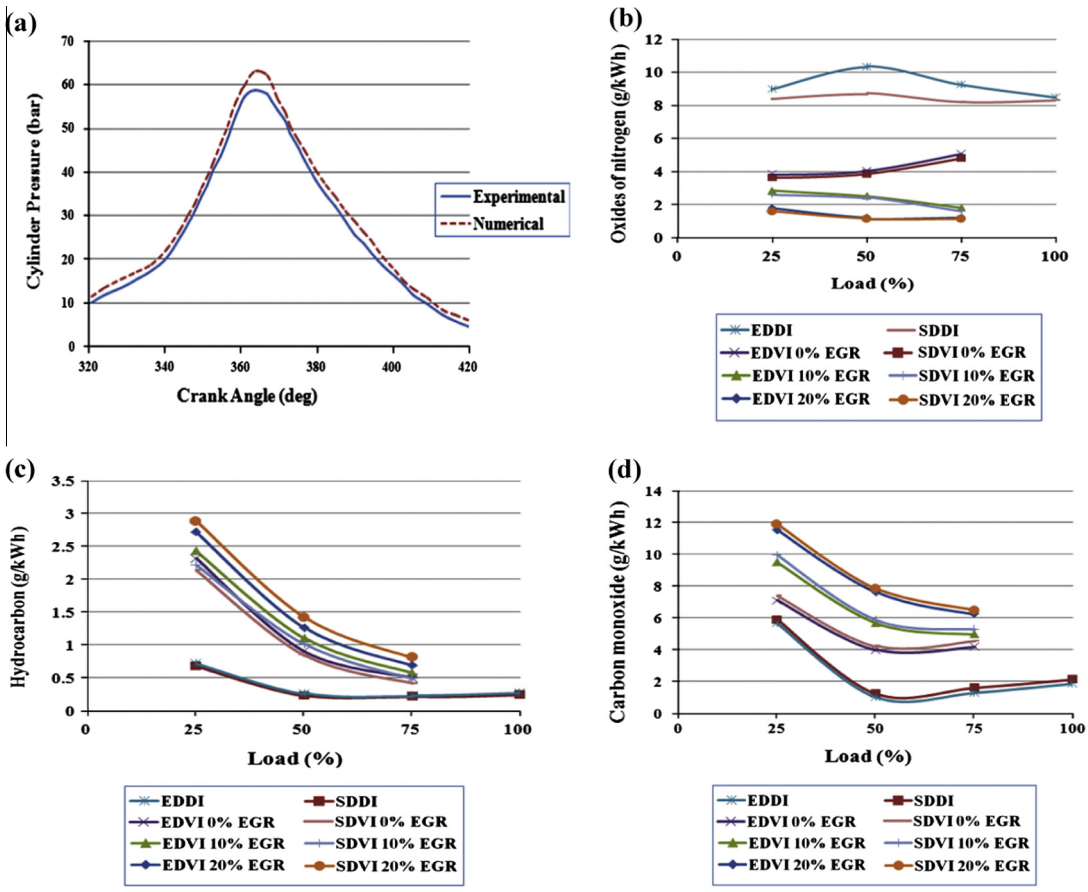

Figure 3 Validation of the ECFM-3Z compression ignition model with the experimental results of external mixture formation of HCCI engine.

$$\frac{d}{dt}[\mathrm{NO}] = 2k_{1f}[\mathrm{O}][\mathrm{N_2}]\left\{\frac{\{1-[\mathrm{NO}]^2/K_{12}[\mathrm{O_2}]\Sigma d_2\}}{1+k_{1b}[\mathrm{NO}]/(k_{2f}[\mathrm{O_2}]+k_{3f}[\mathrm{OH}])}\right\} \tag{14}$$

where $K_{12} = (k_{1f}/k_{1b})(k_{2f}/k_{2b})$ and the subscripts 1, 2 and 3 refer to Eqs. (10)–(12), respectively.

O_2, N_2, O, and OH are assumed to be in local thermodynamic equilibrium.

4.6. EGR modeling

Exhaust Gas Recirculation technique improves the auto-ignition capabilities as it retains some hot combustion gases for the next combustion cycle and also it reduces the NOx emissions.

There are two EGR models as stated below.

(a) Variable composition — it considers and components of EGR called six scalars such as EGR_CO_2, EGR_O_2, EGR_H_2O, EGR_CO, EGR_N_2 and EGR_H_2 which can be solved by transport equations. Out of all the scalars the EGR_O2 scalar does not take part in the reaction.
(b) Fixed composition — in this the mass fraction of each scalar (total sum should be equal to 1) should be entered to define the EGR mixture.

To simulate the EGR model variable composition model is used in the present analysis. Here the EGR is the ratio of the re-circulating exhausts gas mass (m_{egr}) to the total mass of charge that enters the cylinder (m_I).

Thus:

$$egr = \frac{m_{\mathrm{egr}}}{m_I} \tag{15}$$

where

$$m_I = m_{\mathrm{air}} + m_{\mathrm{egr}} + m_f \tag{16}$$

For the Individual species

$$m_{\mathrm{egr}(f)} = \mathrm{egr} \cdot m_{E(f)} \tag{17}$$

$$m_{\mathrm{egr}(\mathrm{O2})} = \mathrm{egr} \cdot m_{E(\mathrm{O2})} \tag{18}$$

$$m_{\mathrm{egr}(\mathrm{CO2})} = \mathrm{egr} \cdot m_{E(\mathrm{CO2})} \tag{19}$$

$$m_{\mathrm{egr}(\mathrm{N2})} = \mathrm{egr} \cdot m_{E(\mathrm{N2})} \tag{20}$$

$$m_{\mathrm{egr}(\mathrm{H2O})} = \mathrm{egr} \cdot m_{E(\mathrm{H2O})} \tag{21}$$

where m_f = mass of the fuel.

The ratio of mass of individual gas to the total mass of all exhaust gases gives the mass fraction of that particular gas.

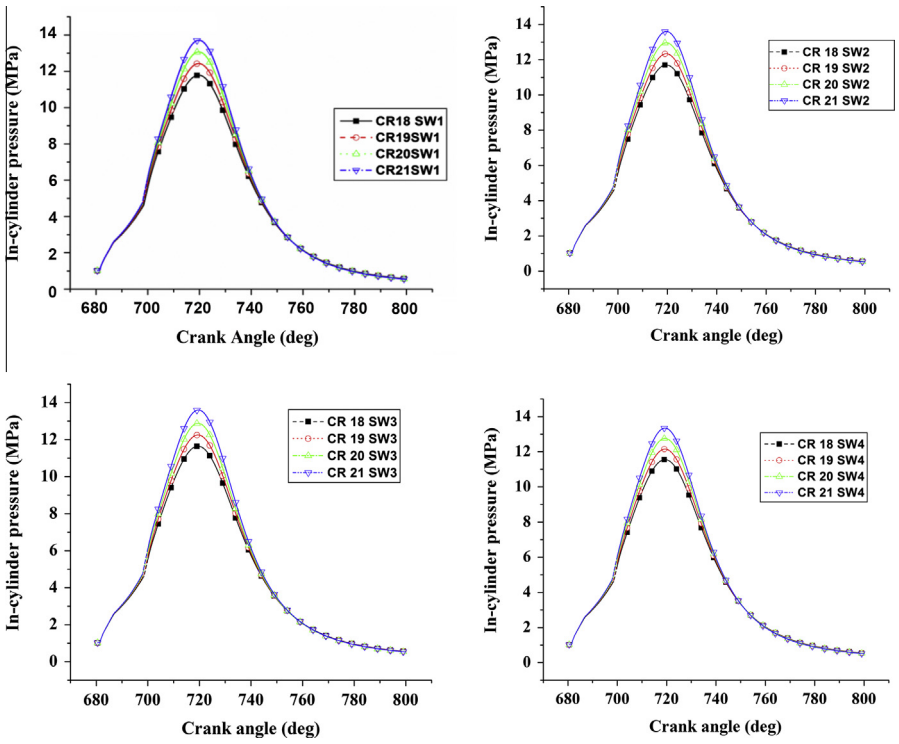

Figure 4 In-cylinder pressure vs Crank angle at different compression ratios and swirl ratios.

Table 3 Peak pressures (MPa) at various compression ratios and swirl ratios.

Compression ratio	SW1	SW2	SW3	SW4	Percentage reduction between SW1 and SW4
CR 18	11.78	11.70	11.64	11.55	1.98
CR 19	12.43	12.33	12.25	12.14	2.27
CR 20	13.06	12.96	12.88	12.75	2.37
CR 21	13.71	13.60	13.47	13.34	2.70
Percentage between CR 18 and CR 21	16.352	16.20	15.73	15.491	

5. Initial and boundary conditions

The initial boundary conditions considered for the analysis are; an absolute pressure of 1.02 bar, 353 K initial temperature, 0% EGR, 0.26 equivalence ratio. Wall temperatures of combustion dome region are fixed as 400 K, dome regions as 450 K and piston crown regions as 450 K. The Angleberger wall function mode [22] is considered. By solving momentum, turbulence and mass equations boundary layers with no-slip are computed by 'two-layer' and low Reynolds number approaches. In the analysis a combined "two layered" and "low Reynolds number" hybrid wall boundary condition is used. The need for using a small value for y^+ was eliminated by the use of hybrid wall boundary condition, which creates very fine mesh near the walls. By using the expression of asymptotic valid for $0.1 < y^+ < 100$ or by combining the low and high Reynolds number expression for chemical species, thermal energy, shear stresses wall fluxes the y^+ independency was achieved along with providing all necessary boundary conditions for a wide range of near-wall mesh densities. The variable values on the wall and at the near wall cells are calculated by using hybrid wall functions.

6. Validation of ECFM-3Z, compression ignition model

Many well established automotive industries and researchers are adopting STAR-CD CFD package for 3 dimensional analyses on IC engines. Many researchers like Pasupathy Venkateswaran and Nagarajan [9], Zellat et al. [23], Bakhshan et al. [24] validated the STAR-CD package with the experimental results and found the good agreement between experimental and model results. In the present analysis the Combustion aspects of a CI engine in HCCI mode were done by using ECFM-3Z model by considering Ganesh and Nagarajan [25] engine specifications to validate the model results. Ganesh et al. conducted experiments in both direct diesel injection mode and diesel vapor induction mode at varying EGR fractions. They developed a fuel vaporizer to evaporate the diesel fuel and to prepare a homogeneous mixture with air before entering into the cylinder. He has compared the engine in-cylinder pressures and emissions in both the cases and found that the diesel vapor induction results are good when compared with the direct diesel injection. Validation of ECFM-3Z model results with Ganesh and Nagarajan [25] experimental results was performed by choosing the same engine boundary conditions and specification.

Graphs of performance and emissions with simulation and experimental values are drawn to examine the variation in results. It was found that the results of ECFM-3Z are in good coherence with the experimental results of Ganesh and

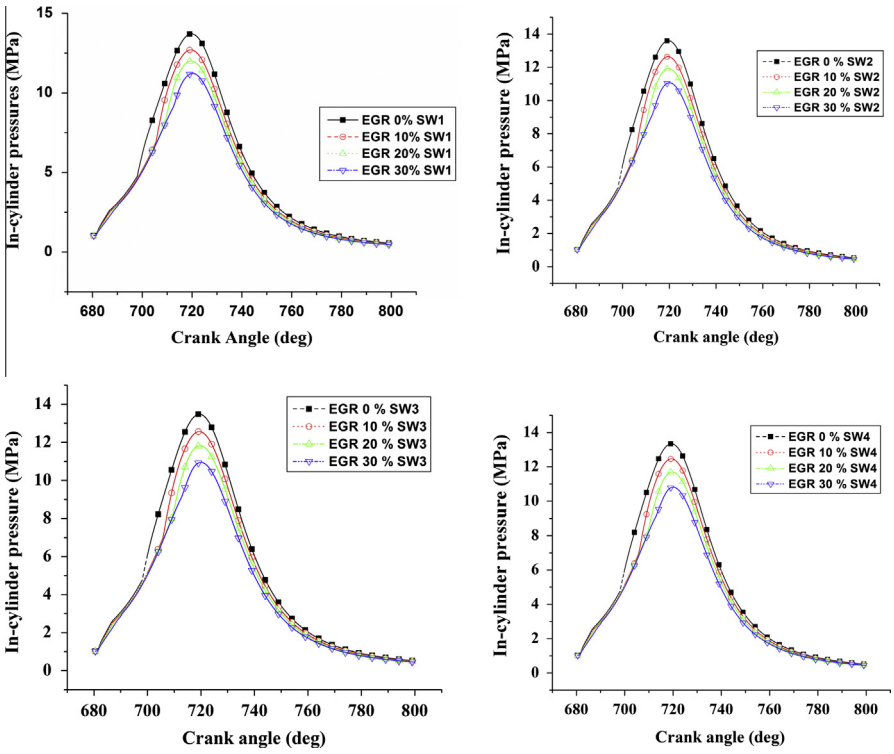

Figure 5 In-cylinder pressure vs Crank angle at different EGR concentrations and swirl ratios.

Table 4 Peak pressures (MPa) at various exhaust gas recirculation and swirl ratios.

EGR (%)	SW1	SW2	SW3	SW4	% Reduction between SW1 and SW4
EGR 0%	13.71	13.60	13.47	13.34	2.70
EGR 10%	12.70	12.63	12.56	12.45	1.94
EGR 20%	12.01	11.92	11.82	11.69	2.58
EGR 30%	11.23	11.06	10.94	10.81	3.72
% Reduction between EGR 0% and EGR 30%	18.096	18.644	18.783	18.953	

Nagarajan [25] and are depicted in Fig. 3. In the figures EDVI – Experimental Diesel Vapor Induction, SDVI – Simulated Diesel Vapor Induction, EDDI – Experimental Direct Diesel Injection and SDDI – Simulated Direct Diesel Injection at respective EGR concentrations. The clear variation between DVI and DDI can be seen in Fig. 3.

The error analysis of the validation of ECFM-3Z with the experimental results was performed. The Error between simulated and experimental results is high in case of direct diesel injection when compared with the diesel vapor induction. In case of in-cylinder pressures a maximum deviation of 7.56% at 363 CA during combustion and a minimum of 1.47% at 348 CA were observed. The maximum deviation during combustion is attributed to assumption of fixed wall temperatures instead of mapping to save computational time and storage. NOx emissions showed a variation of 4.2% at 25% load and 1.82% at 75% load. The error in hydrocarbon emissions was obtained as 5.474% at 25% load and 4.31% at 75% load. In case of CO emissions the error was observed to be 4.69% at 25% load and 8.69% at 75% load. EGR was observed to be a dominant parameter in reducing error in the values of NOx emissions where as the error has increased with HC emissions as the model has over predicted it. No variation in error is observed with EGR in case of CO emissions.

7. Results and discussion

The effect of induction induced swirl in reducing peak pressures has been studied computationally by varying operating parameters such as compression ratio, equivalence ratio, exhaust gas recirculation, and boost pressure. The swirl ratios ranging from 1 to 4 are considered for the analysis. The simulation results of the ECFM-3Z model are discussed below.

7.1. Compression ratio

The variation of peak pressures of the reentrant piston bowl with compression ratio for swirl ratios 1–4 are plotted in Fig. 4. From Table 3, it can be observed that lower compression ratios and higher swirl ratios are favorable in limiting the peak pressures. The peak pressures obtained at different compression ratios and swirl ratios are summarized in Table 3.

The peak in-cylinder pressure increases with compression ratio irrespective of the swirl ratio, but the percentage increase in peak pressures is less at higher swirl ratios [26]. As swirl ratio increases; reduced peak pressures are obtained at all compression ratios, but the decrease in peak pressures is high at higher compression ratios [27]. The reason for this

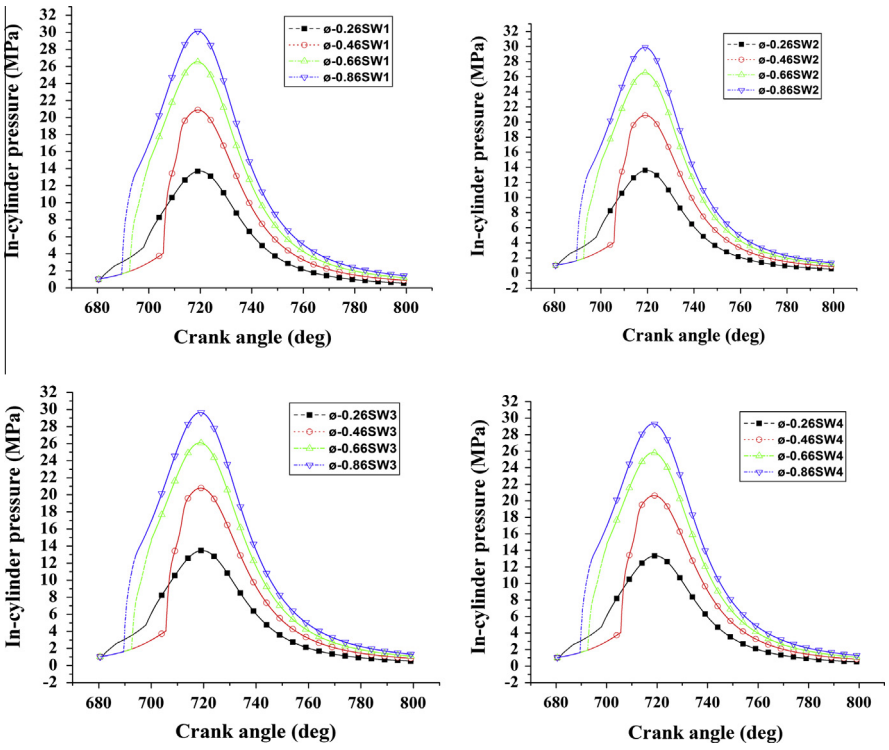

Figure 6 In-cylinder pressure vs Crank angle at different equivalence ratio and swirl ratios.

Table 5 Peak pressures (MPa) at various equivalence ratios and swirl ratios.

EQR	SW1	SW2	SW3	SW4	% Reduction between SW1 and SW4
EQR 0.26	13.71	13.60	13.47	13.34	2.70
EQR 0.46	20.89	20.89	20.79	20.63	1.21
EQR 0.66	26.55	26.55	26.09	25.83	2.71
EQR 0.86	30.14	29.89	29.64	29.32	2.72
% Increase between EQR 0% and EQR 30%	119.708	119.112	120.89	120.300	

phenomenon is increase in turbulence owing to increased wall heat transfer due to increased swirl intensity.

7.2. Exhaust Gas Recirculation (EGR)

The variation of peak pressures of the reentrant piston bowl with EGR concentration with swirl ratios 1–4 are plotted in Fig. 5. From Table 4, it can be observed that higher EGR concentrations and higher swirl ratios are favorable in reducing the peak pressures. The peak pressures obtained at different EGR concentrations and swirl ratios are plotted in Table 4.

The peak pressure decreases with increase in EGR concentration irrespective of the swirl ratio, but percentage reduction in peak pressures is high at higher EGR levels with higher swirl ratios. This can be attributed to release of reduced net energy with decrease in volumetric efficiency of the engine at higher EGR levels and owing to oxygen availability for the combustion process. As swirl ratio increases; lower peak pressures are obtained at any EGR concentration, but percentage reduction in peak pressures is high at higher swirl ratios and higher EGR concentrations. The reason for this phenomenon is increase in turbulence owing to increased wall heat transfer because of increased swirl ratios [28,29]. This study also indicated modest shift in the occurrence of maximum peak pressure towards TDC with increase in EGR concentrations [30].

7.3. Equivalence ratio (ø)

The variation of peak pressures of the reentrant piston bowl with equivalence ratio with swirl ratios 1–4 is plotted in Fig. 6. From Table 5 it can be observed that lower equivalence ratios and higher swirl ratios are favorable in reducing the peak pressures. The peak pressure increases with increase in equivalence ratio irrespective of the swirl ratio, but the percentage increase in peak pressures is marginal at all swirl ratios [31,32]. The reason behind it is increased equivalence ratio injects more fuel leading to rich mixture formation process, combustion of more quantity of fuel leads to increase in peak pressures. As swirl ratio increases; decrease in peak pressures is obtained at all equivalence ratios, but percentage reduction in peak pressures is high at high swirl ratios and lower equivalence ratios. This may again be due to increased turbulence owing to increased wall heat transfer losses because of increased swirl ratios.

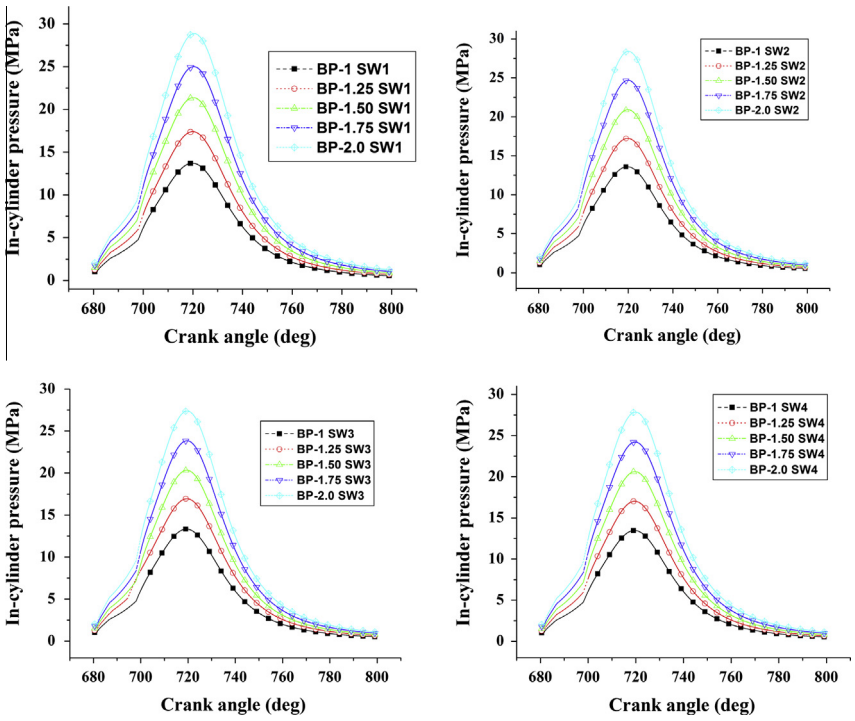

Figure 7 In-cylinder pressure vs Crank angle at different boost pressures and swirl ratios.

Table 6 Peak pressures (MPa) at various boost pressures and swirl ratios.

Boost pressures (bar)	SW1	SW2	SW3	SW4	% Reduction between SW1 and SW4
BP 1.0	13.71	13.60	13.47	13.34	2.70
BTP 1.25	17.39	17.24	17.03	16.95	2.52
BP 1.5	21.37	20.91	20.61	20.32	4.90
BTP 1.75	25.01	24.69	24.21	23.85	4.63
BTP 2.0	28.87	28.39	27.86	27.38	5.16
Percentage increase between BP 1.0 and BP 2.0	110.545	108.777	106.731	105.235	

7.4. Boost Pressure (BP)

The variation of peak pressures of the reentrant piston bowl with boost pressures with swirl ratios 1–4 is plotted in Fig. 7. From Table 6 it can be observed that lower boost pressures and higher swirl ratios are favorable in mitigating the peak pressures. The peak pressures increase with increase in boost pressures irrespective of the swirl ratio, but the percentage increase in peak pressures is less at higher swirl ratios [33,34]. As swirl ratio increases; lower peak pressures are obtained at any boost pressure, but the percentage decrease in peak pressures is high at higher boost pressures. The reason for this phenomenon is increase in turbulence owing to increased wall heat transfer losses because of increased swirl ratios.

8. Conclusions

High in-cylinder peak pressures of HCCI engine due to volumetric combustion may damage the engine and thereby demands a rigid engine construction. A computational analysis is undertaken to find the impact of induction induced swirl in lowering peak pressures of HCCI engine. A study has been attempted using Extended Coherent Flame combustion model for peak pressure reduction of a HCCI engine with induced swirl motion under different operating conditions. The present investigation disclosed that ECFM-3Z of STAR-CD is well suitable for HCCI mode of combustion with necessary modifications, in coherence with the existing literature. It was found that swirl ratio has a considerable impact in limiting the peak pressures of HCCI engine. The analysis resulted in achieving about 21% reduction in peak pressures when a swirl ratio of 4 with 30% EGR is adopted when compared to a swirl ratio of 1 with 0% EGR. The effect of four operating parameters viz; compression ratio, exhaust gas recirculation, equivalence ratio and boost pressure under varying swirl ratios suggested lower compression ratios, higher EGR concentrations, lower equivalence ratios, lower boost pressures and higher swirl ratios are favorable in reducing the peak pressures. The study revealed that adoption of high swirl ratios associated with high EGR levels would lead to significant reduction in peak pressures in HCCI mode.

Acknowledgements

The authors thank Dr. Raja Banerjee, Associate Professor, IIT Hyderabad for allowing to use computational facility, Mr. B. Siva Nageswara Rao from CD-adapco, Bengaluru and Mr. P. Madhu computer Laboratory supervisor IIT Hyderabad for their support during the simulation work.

References

[1] T. Karthikeya Sharma, G. Amba Prasad Rao, K. Madhu Murthy, Performance of HCCI diesel engine under the influence of various working and geometrical parameters, Int. J. Theor. Appl. Res. Mech. Eng. 1 (2012) (2012) 2319–3182.

[2] K. Epping, S. Aceves, R. Bechtold, J.E. Dec, The potential of HCCI Combustion for High Efficiency and Low Emissions (No. 2002-01-1923), SAE Technical Paper, 2002.

[3] B. Liu, W. Su, H. Wang, H. Huang, Characteristics and energy distribution of modulated multi-pulse injection modes based diesel HCCI combustion and their effects on engine thermal efficiency and emissions, Front. Energy Power Eng. Chin. 1 (4) (2007) 420–427.

[4] J.B. Heywood, Internal Combustion Engine Fundamentals, McGraw-Hill Inc., New York, NY, 1988, ISBN 0-07-028637-X.

[5] S. Onishi, S.H. Jo, K. Shoda, P.D. Jo, S. Kato, Active Thermo-Atmosphere Combustion (ATAC) – A New Combustion Process for Internal Combustion Engines, SAE Paper 790501, 1979.

[6] T. Karthikeya Sharma, G. Amba Prasad Rao, K. Madhumurthy, Combustion analysis of ethanol in HCCI engine, Trends Mech. Eng. 3 (1) (2012).

[7] Gen Chen, Norimasa Iida, Zuohua Huang, Numerical study of EGR effects on reducing the pressure rise rate of HCCI engine combustion, Front. Energy Power Eng. Chin. 4 (3) (2010) 376–385.

[8] R. Manimaran, R. Thundil Karuppa Raj, Computational studies of swirl ratio and injection timing on atomization in a direct injection diesel engine, Front. Heat Mass Transfer (FHMT) 5 (1) (2014).

[9] S.P. Venkateswaran, G. Nagarajan, Effects of the re-entrant bowl geometry on a DI turbocharged diesel engine performance and emissions—a CFD approach, J. Eng. Gas Turbines Power 132 (12) (2010) 122803.

[10] F. Maroteaux, L. Noel, A. Ahmed, Numerical investigations on methods to control the rate of heat release of HCCI combustion using reduced mechanism of n-heptane with a multidimensional CFD code, Combust. Theor. Model. 11 (4) (2007) 501–525.

[11] J.P. Duclos, M. Zolver, T. Baritaud, 3D modeling of combustion for DI–SI engines, Oil Gas Sci. Technol. 54 (2) (1999) 259–264.

[12] O. Colin, A. Benkenida, The 3-Zone Extended Coherent Flame Model (ECFM3Z) for computing premixed/diffusion combustion, Oil Gas Sci. Technol. – Rev IFP 59 (6) (2004) 593–609.

[13] D. Abouri, M. Zellat, S. Duranti, F. Ravet, Advances in combustion modeling in STAR-CD: validation of ECFM CLE-H model to engine analysis, in: 18th International Multidimensional Engine User's Meeting at the SAE Congress, 2008.

[14] G. Subramanian, L. Vervisch, F. Ravet, New Developments in Turbulent Combustion Modeling for Engine Design: ECFM-CLEH Combustion sub-model (No. 2007-01-0154), SAE Technical Paper, 2007.

[15] K.Y. Huh, A.D. Gosman, A phenomenological model of Diesel spray atomization, in: Proc. Int. Conf. on Multiphase Flows (ICMF '91), Tsukuba, 24–27 September, 1991.

[16] C. Bai, A.D. Gosman, Development of Methodology for Spray Impingement Simulation, SAE Technical Paper Series, SAE Paper No. 950283, 1995.

[17] R.D. Reitz, R. Diwakar, Structure of High-Pressure Fuel Spray, SAE Technical Paper Series, SAE Paper No. 870598, 1987.

[18] R.D. Reitz, R. Diwakar, Effect of Drop Breakup on Fuel Sprays, SAE Technical Paper Series, SAE Paper No. 860649, 1986.

[19] C. Angelberger, T. Poinsot, B. Delhay, Improving Near-Wall Combustion and Wall Heat Transfer Modeling in SI EngineComputations, SAE Technical Paper Series 972881, 1997, pp. 113–130.

[20] M.A. Patterson, S.-C. Kong, G.J. Hampson, R.D. Reitz, Modeling the Effects of Fuel Injection Characteristics on Diesel Engine Soot and NOx Emissions, SAE Paper 940523, 1994.

[21] J.B. Heywood, Internal Combustion Engine Fundamentals, McGraw-Hill Company, 1988.

[22] V. Moureau, G. Lartigue, Y. Sommerer, C. Angelberger, O. Colin, T. Poinsot, Numerical methods for unsteady compressible multi-component reacting flows on fixed and moving grids, J. Comput. Phys. 202 (2) (2005) 710–736.

[23] M. Zellat, S. Duranti, Y. Liang, C. Kralj, G. Schmidt, J.M. Duclos, Toward a universal combustion model in STAR-CD for IC engines: from GDI to HCCI and application to DI Diesel combustion optimization, in: Proceedings of 14th International Multidimensional Engine User's Meeting, SAE Cong, 2005.

[24] Y. Bakhshan et al, Multi-dimensional simulation of n-heptane combustion under HCCI engine condition using detailed chemical kinetics, J. Engine Res. 22 (Spring) (2011).

[25] D. Ganesh, G. Nagarajan, Homogeneous charge compression ignition (HCCI) combustion of diesel fuel with external mixture formation, Energy 35 (1) (2010) 148–157.

[26] A. Viggiano, V. Magi, A comprehensive investigation on the emissions of ethanol HCCI engines, Appl. Energy 93 (2012) 277–287.

[27] R. Song, T. Hu, L. Zhou, S. Liu, W. Li, Effects of compression ratio on the combustion characteristics of a homogeneous charge compression ignition engine, Front. Energy Power Eng. Chin. 1 (4) (2007) 463–467.

[28] Y. Gu, J.R. Mayor, W.J.A. Dahm, Turbulence-augmented minimization of combustion time in mesoscale internal combustion engines, in: 44th AIAA Aerospace Sciences Meeting and Exhibit, AIAA-2006-1350.

[29] G. Chen, N. Iida, Z. Huang, Numerical study of EGR effects on reducing the pressure rise rate of HCCI engine combustion, Front. Energy Power Eng. Chin. 4 (3) (2010) 376–385.

[30] B. Krishna, Murali, J.M. Mallikarjuna, Effect of engine speed on peak tumble flows in a motored internal combustion engine – an experimental investigation using particle image velocimetry, J. Appl. Fluid Mech. 4.1: 1-14-2011.

[31] J. Martinez-Frias, S.M. Aceves, D. Flowers, J.R. Smith, R. Dibble, Equivalence Ratio-EGR Control of HCCI Engine Operation and the Potential for Transition to Spark-ignited Operation (No. 2001-01-3613), SAE Technical Paper, 2001.

[32] M. Christensen, B. Johansson, Influence of mixture quality on homogeneous charge compression ignition, J. Fuels Lubricants (1998) 107, SAE Transactions.

[33] J.O. Olsson, P. Tunestål, B. Johansson, Boosting for High Load HCCI (No. 2004-01-0940), SAE Technical Paper, 2004.

[34] M. Christensen, B. Johansson, P. Amnéus, F. Mauss, Supercharged Homogeneous Charge Compression Ignition (No. 980787), SAE Technical Paper, 1998.